Editors' Suggestion

Radio-Frequency Manipulation of State Populations in an Entangled Fluorine-Muon-Fluorine System

David Billington,[1,*] Edward Riordan,[1] Majdi Salman,[1] Daniel Margineda,[1] George J. W. Gill,[1] Stephen P. Cottrell,[2] Iain McKenzie,[3] Tom Lancaster,[4] Michael J. Graf,[5] and Sean R. Giblin[1,†]

[1]School of Physics and Astronomy, Cardiff University, Queen's Building, The Parade, Cardiff CF24 3AA, United Kingdom
[2]ISIS Facility, Rutherford Appleton Laboratory, Harwell Campus, Didcot, Oxon OX11 0QX, United Kingdom
[3]TRIUMF, Vancouver, British Columbia V6T 2A3, Canada
[4]Department of Physics, Centre for Materials Physics, Durham University, Durham DH1 3LE, United Kingdom
[5]Department of Physics, Boston College, Chestnut Hill, Massachusetts 02467, USA

(Received 13 April 2022; accepted 12 July 2022; published 9 August 2022)

Entangled spin states are created by implanting muons into single-crystal $LiY_{0.95}Ho_{0.05}F_4$ to form a cluster of correlated, dipole-coupled local magnetic moments. The resulting states have well-defined energy levels allowing experimental manipulation of the state populations by electromagnetic excitation. Experimental control of the evolution of the muon spin polarization is demonstrated through application of continuous, radio-frequency electromagnetic excitation fields. A semiclassical model of quantum, dipole-coupled spins interacting with a classical, oscillating magnetic field accounts for the muon spin evolution. On application of the excitation field, this model shows how changes in the state populations lead to the experimentally observed effects, thus enabling a spectroscopic probe of entangled spin states with muons.

DOI: 10.1103/PhysRevLett.129.077201

The preparation, manipulation, and measurement of entangled quantum states lies at the heart of emerging quantum technologies. There are numerous methods for creating entangled states, where the manipulation is enabled by electromagnetic pumping at a frequency corresponding to the interval between the energy levels. One such entangled state often occurs when a positively charged, 100% spin-polarized muon, μ^+, is implanted into a material containing fluorine. The stopped μ^+ tends to form hydrogen-like bonds with two nearby F^- ions forming a linear (180° bond angle) F—μ—F complex. Magnetic dipole coupling between the μ^+ spin ($S = 1/2$) and the two F^- nuclear spins ($I = 1/2$) produces four doubly degenerate, so-called F—μ—F energy eigenstates [1–3]. The resulting μ^+ spin polarization, as measured by muon spin relaxation (μ^+SR), evolves over time because the initial state of the system is, essentially, a statistical mixture of superpositions of (typically) nondegenerate energy eigenstates, and it exhibits oscillations driven by the magnetic dipole coupling between the entangled moments comprising the F—μ—F states [4].

In recent years, there has been significant effort to increase the decoherence time of entangled states, as this is an obstacle to enhanced quantum technologies. In general, the environment of a quantum system acts as a source of decoherence [5], where the initial quantum information describing the system leaks into the environment and can no longer be recovered. Recently, the decoherence of the entangled F—μ—F states was successfully modeled by considering interactions with the *local* (nearest-neighbor) magnetic moments of the F—μ—F complex [6,7], demonstrating that the F—μ—F states are robust and well isolated from other, *external* environmental dephasing mechanisms. In this Letter, we demonstrate experimental control of the evolution of the μ^+ spin polarization in single-crystal $LiY_{0.95}Ho_{0.05}F_4$ and demonstrate that the spin system is effectively isolated from the external environment over the lifetime of the measurement, thus enabling the experimental manipulation of entangled state populations. Control of the transitions between the entangled spin states is achieved simply by *in situ* radio frequency (RF) electromagnetic excitation within the μ^+SR sample environment. Previous RF-μ^+SR experiments [8,9] have generally focused on either decoupling the μ^+ spin from its local environment [10,11] or exploiting the bipartite muonium system (which can couple to its local environment) in order to investigate, for example, local coupling constants [12,13]. In contrast, here the RF excitation field is applied continuously to drive transitions between the entangled F—μ—F states. Although there are more precise ways of manipulating state populations through the careful timing and shaping of RF pulses, the continuous application of the RF field is shown to be sufficient for this proof-of-principle experiment.

The initial states are created by implanting 100% spin-polarized μ^+ into single-crystal $LiY_{0.95}Ho_{0.05}F_4$, where they predominantly stop near two F^- ions and form entangled states similar to the F—μ—F states. We used a previously studied large single crystal of $LiY_{0.95}Ho_{0.05}F_4$ [14], which has a tetragonal structure that is essentially unchanged from the parent $LiYF_4$ and is known to have more than 80% of the implanted μ^+ form entangled states. While the Ho^{3+} ion is strongly magnetic, in $LiY_{1-x}Ho_xF_4$ it was shown that the dipole-coupled oscillations at $T = 50$ K were independent of Ho^{3+} concentration for $0.002 \leq x \leq 0.086$ [14], demonstrating that the Ho^{3+} magnetic moments are fluctuating very rapidly and are thus on a timescale far outside the μ^+ time window, so they will have a negligible effect on the measurements reported here.

To demonstrate experimentally how the μ^+ polarization is sensitive to the population of the underlying eigenstates, and that we can manipulate and observe changes in these populations, μ^+SR spectra were measured using the EMU spectrometer [15] at the STFC-ISIS facility in the UK. The μ^+ spin was initially polarized along $+z$, and the RF coil was oriented such that the RF excitation field, $\boldsymbol{B}(t) = [0, B_y \cos(\omega_c t), 0]$, was linearly polarized along y (perpendicular to the incoming μ^+ beam, z) with the $LiY_{0.95}Ho_{0.05}F_4$ single crystal aligned with its c axis along the field axis [see Fig. 1(a)]. All of our measurements were performed at temperature $T = 50$ K with zero static $\boldsymbol{B}$ field. Only the oscillating $\boldsymbol{B}(t)$ was applied continuously over about 15 μ^+ lifetimes (about 33 μs, the lifetime of the measurement) using a RF saddle coil in close proximity to the sample (details in the Supplemental Material [16]). A nominal excitation frequency $[\omega_{on}/(2\pi) = 550$ kHz] was chosen to match the highest-energy transition between the energy levels of the F—μ—F states [see Fig. 1(c)], which hereafter we refer to as the on-resonance condition. Spectra were measured both on and off $[\omega_{off}/(2\pi) = 825$ kHz] the resonance condition and, for each RF frequency, data were collected alternately with (RF-on, $B_y \neq 0$) and without (RF-off, $B_y = 0$) the applied excitation field for 500 accelerator pulses each, where each pulse duration is about 80 ns (full width at half maximum).

To determine the μ^+ stopping site and associated local structural distortion within the crystal [6,7,17], first-principles calculations [18–20] were performed. We found a unique minimum-energy structural configuration in which the two nearest neighbors of the μ^+ are both F^- ions (forming a state resembling F—μ—F), the two next-nearest-neighbors are both Li^+ ions, and the two next-next-nearest-neighbors are both F^-. Together, these comprise a $\mu F_2Li_2F_2$ cluster, as shown in Fig. 1(b). There are 16 symmetry-equivalent positions within the tetragonal structure; however, since rotations of the F—μ—F bonds about the z axis (initial μ^+ spin direction) do not affect the observed μ^+ polarization, there are only two orientations (rotated by 90° about the c axis) of the crystallographically equivalent μ^+ stopping site to consider. The calculations show that the F^- ions and Li^+ ions move towards and away from the μ^+ site, respectively, to minimize the electrostatic energy. Table S1 in Ref. [16] lists the calculated atomic positions for the two orientations of the μ^+ stopping site.

To model the decoherence of the F—μ—F states in $LiY_{0.95}Ho_{0.05}F_4$, magnetic dipole interactions with the

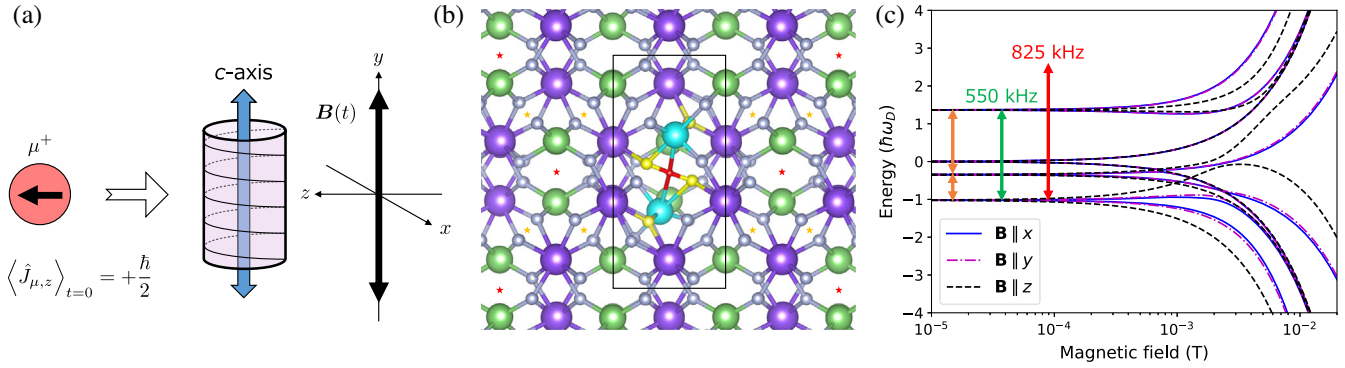

FIG. 1. (a) Schematic of the experimental geometry. (b) Crystal structure of $LiYF_4$ in the tetragonal ac plane (experimental zy plane) with the Li^+ (green), Y^{3+} (purple), and F^- (gray) ions shown as spheres. The calculated μ^+ stopping site (red) and associated structural distortion (described in the main text) are shown in the center. Highlighted are the two nearest-neighbor F^- ions (yellow), the two next-nearest-neighbor Li^+ ions (cyan), and the two next-next-nearest-neighbor F^- ions (yellow) of μ^+ which are included in the $\mu F_2Li_2F_2$ cluster calculation and whose positions are most affected by the structural distortion. Other crystallographically equivalent μ^+ stopping sites are indicated by red and orange stars for sites with the same $\mu F_2Li_2F_2$ atomic geometry as the one shown and for sites with the same atomic geometry but rotated by 90° about the c axis, respectively. The black rectangle is the tetragonal unit cell. (c) Energy-level diagram of an isolated F—μ—F complex with the same orientation shown in (b) as a function of the magnetic field. For small $\boldsymbol{B}$ fields, three transitions are possible (orange and green double-ended arrows). The 550 kHz transition (green) used in this experiment is highlighted, along with an 825 kHz excitation (red) which is also used, but, importantly, does not correspond to a transition. For the μ^+ stopping sites indicated by orange stars in (b), x and z are exchanged in (c).

two next-nearest Li^+ and two next-next-nearest F^- ions must be included. From the calculated geometry, we construct and optimize [21] a dipole interaction Hamiltonian for a $\mu F_2Li_2F_2$ cluster, to which we add a term representing the interaction of the spins with an oscillating magnetic field, $\boldsymbol{B}(t)$, with frequency equal to the level separation. Utilizing the Quantum Toolbox in Python (QuTiP) module [22,23], we then evolve the initial density matrix according to our optimized Hamiltonian and evaluate the expectation value of the z-direction μ^+ spin projection operator, $\langle \hat{J}_{\mu,z} \rangle(t)$.

The only stable isotope of fluorine is ^{19}F [$I = 1/2$, $\gamma_F/(2\pi) = 40.053\ \mathrm{MHz\,T^{-1}}$], and the stable isotopes of lithium are ^6Li [$I = 1$, $\gamma_{^6Li}/(2\pi) = 6.2661\ \mathrm{MHz\,T^{-1}}$] and ^7Li [$I = 3/2$, $\gamma_{^7Li}/(2\pi) = 16.548\ \mathrm{MHz\,T^{-1}}$], which occur with relative abundances of 7.42% and 92.58%, respectively. Because ^7Li is much more abundant and the gyromagnetic ratio of ^6Li is about 2/3 smaller, only ^7Li is considered in our model. The initial density matrix for the $\mu F_2Li_2F_2$ cluster, $\hat{\rho}_{\mu F_2Li_2F_2}(t=0)$, is given by the tensor product of the initial density matrices of the seven subsystems. Except for μ^+, which is initially polarized in the $|\uparrow\rangle$ state, all of the other initial density matrices are (in the $\hat{J}_z$ basis) identity matrices weighted with equal probability, $\hat{\rho}_{i\neq\mu}(0) = \mathbb{I}_{d_i}/d_i$, where $d_i = 2j_i + 1$ is the dimension of the ith subsystem with total angular momentum quantum number j_i. The identity matrices represent the maximally mixed (equal-probability) states of the nuclear spin moments of the $^{19}F^-$ ($I = 1/2$) and $^7Li^+$ ($I = 3/2$) ions, which, together with μ^+ ($S = 1/2$), give a total number of states, $N_s = \prod_{i=1}^{N_m} d_i = 512$ for each of the two orientations of the $\mu F_2Li_2F_2$ cluster [red and orange stars in Fig. 1(b)]. The model Hamiltonian is determined by considering a system of N_m magnetic moments coupled via long-range magnetic dipole interactions,

$$\hat{H}_0 = \frac{1}{2}\sum_{i\neq j}^{N_m} \frac{\mu_0\gamma_i\gamma_j}{4\pi|\boldsymbol{r}_{ij}|^3}\left[\hat{\boldsymbol{J}}_i\cdot\hat{\boldsymbol{J}}_j - 3(\hat{\boldsymbol{J}}_i\cdot\boldsymbol{n}_{ij})(\hat{\boldsymbol{J}}_j\cdot\boldsymbol{n}_{ij})\right], \quad (1)$$

where $\boldsymbol{r}_{ij} = \boldsymbol{r}_i - \boldsymbol{r}_j$ are the position vectors connecting moments i and j, μ_0 is the vacuum permeability, γ_i are the gyromagnetic ratios, $\hat{\boldsymbol{J}}_i = (\hat{J}_{i,x}, \hat{J}_{i,y}, \hat{J}_{i,z})$ are the angular momentum vector operators, $\boldsymbol{n}_{ij} = \boldsymbol{r}_{ij}/|\boldsymbol{r}_{ij}|$, and the prefactor (1/2) avoids double counting. Quadrupolar coupling to nuclear spins with $I \geq 1$ from finite electric field gradients has recently been discussed in detail [24,25]; however, these interactions have been neglected in our model, since they are relatively weak for ^7Li ($I = 3/2$) and so will only affect the μ^+ polarization at longer times [6,7].

For the simpler case of a F—μ—F complex, we need only consider the spin of the implanted μ^+ and the two F^- nuclear spins. The energy-level spectrum and allowed transitions are shown in Fig. 1(c) in units of $\hbar\omega_D = \hbar^2\mu_0\gamma_\mu\gamma_F/(4\pi\bar{r}^3_{\mu F})$, where $\bar{r}_{\mu F} \approx 1.2$ Å is the average nearest-neighbor μ–F bond length. The magnetic-field dependence of the F—μ—F eigenstate energies is determined by diagonalizing the Hamiltonian $\hat{H} = \hat{H}_0 + \hat{H}_1$, where $\hat{H}_1 = -\sum_{i=1}^{N_m} \hat{\boldsymbol{\mu}}_i \cdot \boldsymbol{B}$ is the sum of Zeeman interactions between the ith magnetic moment, $\hat{\boldsymbol{\mu}}_i = \gamma_i\hat{\boldsymbol{J}}_i$, and the applied magnetic field, $\boldsymbol{B}$. For $\boldsymbol{B} = 0$, the energy eigenstates exist as doubly degenerate pairs, because a state with all of its spins reversed has the same energy. However, one member of each pair is more and the other less likely to be populated, because μ^+ is initially polarized in the $|\uparrow\rangle$ state. The eigenstate vectors of a dipole-coupled, linear (180°), equidistant F—μ—F complex are listed in Eq. (S3) of Ref. [16]. The on-resonance transitions we are driving can then be written as

$$\begin{aligned}
|\uparrow\uparrow\uparrow\rangle &\rightleftharpoons \left(\frac{3-\sqrt{3}}{12}\right)^{\frac{1}{2}}[(1+\sqrt{3})|\downarrow\uparrow\uparrow\rangle + |\uparrow\uparrow\downarrow\rangle + |\uparrow\downarrow\uparrow\rangle];\\
|\downarrow\downarrow\downarrow\rangle &\rightleftharpoons \left(\frac{3-\sqrt{3}}{12}\right)^{\frac{1}{2}}[(1+\sqrt{3})|\uparrow\downarrow\downarrow\rangle + |\downarrow\downarrow\uparrow\rangle + |\downarrow\uparrow\downarrow\rangle], \quad (2)
\end{aligned}$$

where the first spin in each ket label corresponds to μ^+ and the spin-quantization axis is parallel to the F—μ—F bond axis. Note that the eigenstates on the right-hand side of Eq. (2) are not separable (cannot be written as a tensor product of individual spin states, $|abc\rangle \neq |a\rangle \otimes |b\rangle \otimes |c\rangle$) meaning that the μ^+ spin and two F^- nuclear spins are entangled and, by resonantly driving transitions of this type, we are properly manipulating entangled state populations. The energy-level structure of the $\mu F_2Li_2F_2$ cluster strongly resembles that of the F—μ—F complex, but it appears broadened by the influence of the other moments included in the cluster. To prevent significant perturbation to the F—μ—F energy levels, the applied excitation always has magnetic field amplitude $0.15 \leq B_y \leq 0.30$ mT [see Fig. 1(c)].

For a system interacting with a time-dependent magnetic field, $\boldsymbol{B}(t) = [0, B_y\cos(\omega_c t), 0]$, we have $\hat{H}(t) = \hat{H}_0 + \hat{H}_1(t)$, which is the semiclassical, driven Hamiltonian that we employ to evolve (according to the Liouville–von Neumann equation) the initial density matrix to obtain $\hat{\rho}_{\mu F_2Li_2F_2}(t)$, from which we can calculate the μ^+ spin polarization for each of the $n = 2$ cluster orientations, $P^{\mathrm{calc},n}_{\mu,z}(t)$, given by

$$\left(\frac{\hbar}{2}\right)P^{\mathrm{calc},n}_{\mu,z}(t) = \langle \hat{J}_{\mu,z}\rangle(t) = \mathrm{Tr}[\hat{\rho}^n_{\mu F_2Li_2F_2}(t)\hat{J}_{\mu,z}], \quad (3)$$

where the factor of $\hbar/2$ is to convert the expectation value of the z-direction μ^+ spin projection operator to a dimensionless polarization. The calculated polarization to be compared with the experiment is then the average of

the two orientations, $P^{\mathrm{calc}}_{\mu,z}(t) = [P^{\mathrm{calc},1}_{\mu,z}(t) + P^{\mathrm{calc},2}_{\mu,z}(t)]/2$. The asymmetry function, $A^{\mathrm{fit}}_{\mu,z}(t)$, which we fit to the experimental data, is

$$A^{\mathrm{fit}}_{\mu,z}(t) = A_0 P^{\mathrm{calc}}_{\mu,z}(t) + A_1 \exp(-\lambda_1 t) + A_2, \qquad (4)$$

where $A_0 = 18.5\%$, $A_1 = 3.4\%$, $\lambda_1 = 0.48\ \mu\mathrm{s}^{-1}$, and $A_2 = -1.2\%$ are the results of simultaneously fitting our model to the $\omega_{\mathrm{on}}/(2\pi) = 550$ kHz RF-on ($B_y \neq 0$) and RF-off ($B_y = 0$) experimental spectra (further details in Ref. [16]). The exponential component only contributes to a fast initial depolarization of the spectra and comes from μ^+ not forming F—μ—F within the sample, while the small negative value of A_2 occurs because the inclusion of the RF coil within the μ^+SR sample environment introduces a constant background asymmetry between the forwards and backwards detectors. Except for the excitation frequency, the same set of parameters were used to calculate the μ^+ asymmetry for $\omega_{\mathrm{off}}/(2\pi) = 825$ kHz (see Ref. [16]).

Figure 2 shows the experimental and calculated time evolution of the μ^+ asymmetry for both RF-on and RF-off measurements at $\omega_{\mathrm{on}}/(2\pi) = 550$ kHz and $\omega_{\mathrm{off}}/(2\pi) = 825$ kHz. Additionally, the calculated μ^+ polarization for an isolated F—μ—F complex with the same tetragonal geometry as the $\mu F_2Li_2F_2$ cluster is shown both with and without the driving term, $\hat{H}_1(t)$, demonstrating the decoherence effect of including the *local* environment (additional Li^+ and F^- moments in the $\mu F_2Li_2F_2$ cluster) [6,7]. In terms of the calculations, the combination of muon-site determination, consideration of the μ^+ local environment, and the quantum evolution of an appropriate initial density matrix are essential for describing our experimental data.

Figures 2(c) and 2(d) show the experimental and calculated differences between the RF-on and RF-off measurements at the same RF-field frequencies as Figs. 2(a) and 2(b), respectively. There is clearly a significant change in experimental μ^+ asymmetry at the on-resonance excitation frequency compared to the off-resonance frequency. Crucially, the observed difference in the spectra cannot be caused by a simple change in relaxation rate, which strongly supports the claim that we are measuring a modification of state populations and not simply the periodic redistribution of the eigenstate energies by the oscillating $\boldsymbol{B}(t)$. Importantly, only the first term in Eq. (4) (which is sensitive to the modified eigenstate populations) contributes to the calculated differences. Since our model Hamiltonian is time dependent, the

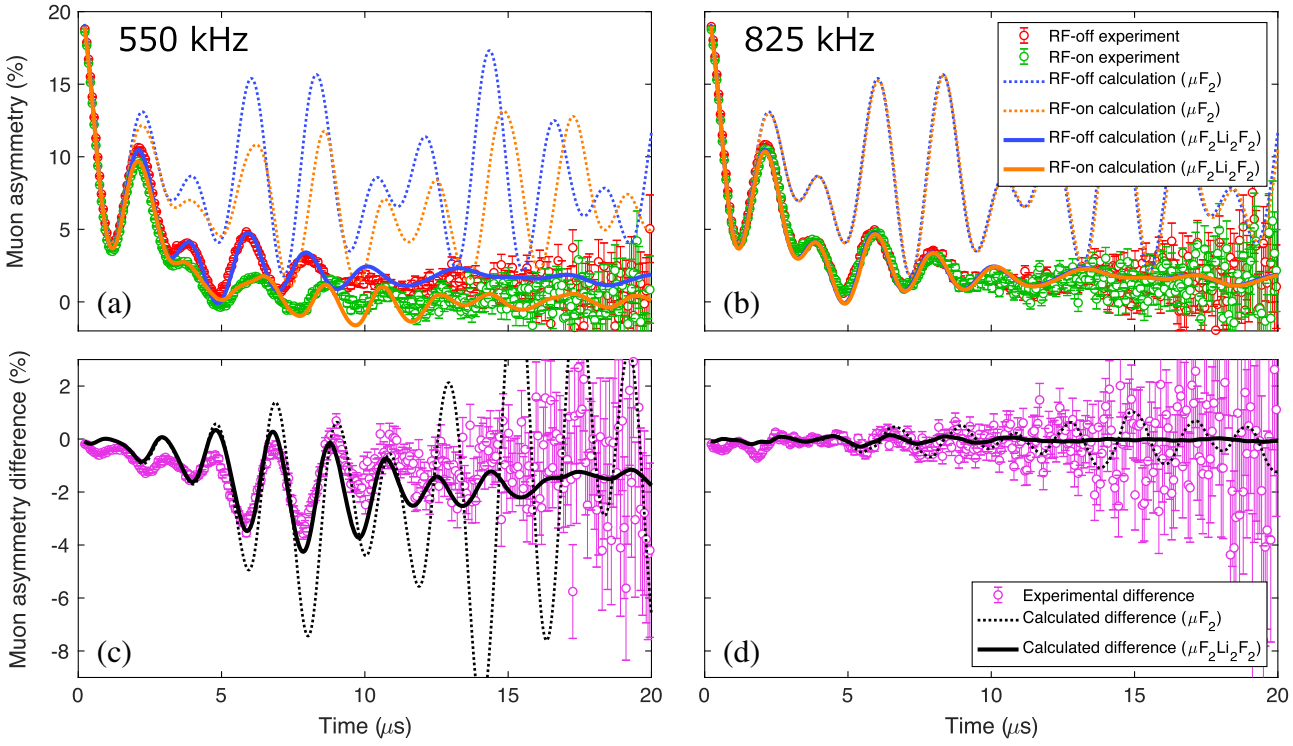

FIG. 2. Experimental μ^+ asymmetry for $LiY_{0.95}Ho_{0.05}F_4$ at $T = 50$ K for both RF-on and RF-off, at excitation frequencies of (a) $\omega_{\mathrm{on}}/(2\pi) = 550$ kHz and (b) $\omega_{\mathrm{off}}/(2\pi) = 825$ kHz, together with those calculated for the F—μ—F complex (μF_2) and the $\mu F_2Li_2F_2$ cluster. The improved agreement with experiment from accurately modeling the decoherence effect (by including the local environment of the F—μ—F complex to form the $\mu F_2Li_2F_2$ cluster) is evident. (c),(d) Experimental and calculated differences between the RF-on and RF-off μ^+ asymmetries in (a) and (b), respectively. Importantly, the on-resonance asymmetry difference cannot be caused by a simple change in relaxation rate.

transitions are between states separated in energy by $\hbar\omega_c$, and thus, any structure in the off-resonance [$\omega_{off}/(2\pi) = 825$ kHz] calculated difference [Fig. 2(d)] is simply related to the periodic degeneracy lifting, because none of the states in our model are separated by energy $\hbar\omega_{off}$ at any time. Figure 2 shows how μ^+, coupled via the magnetic dipole interaction to its local environment, is sensitive to the manipulation of the energy eigenstate populations.

Typically, entangled quantum states lose coherence because of dissipative interactions with the environment [5]. In our case, there is no dissipation involving Lindblad operators or *ad hoc* exponential decay applied to the calculated μ^+ spin polarization, meaning we have created a quantum-entangled spin system that is effectively isolated because the μ^+ spin couples very weakly to its *external* environment over the lifetime of the measurement, owing to the small energy differences involved. When the implanted μ^+ stops in the sample, the magnetic dipole interactions entangle the μ^+ spin with the other nuclear spins of the cluster, which correlates their behavior. This allows the μ^+ quantum information to be decohered into the *local* environment (subsystem of nuclear spins), with the experimentally observable consequence that the μ^+ spin polarization is lost after about 10 μs as the pure (polarized) $|\uparrow\rangle$ state evolves into a mixed (unpolarized) state [5,6]. Nevertheless, the quantum state of the $\mu F_2Li_2F_2$ cluster maintains coherence over the lifetime of the measurement, and thus, our experiment is properly manipulating entangled state populations by resonantly driving transitions.

In conclusion, we have employed a dual experimental and computational approach to probe, manipulate, and model the populations of entangled quantum states in a system of spins that we excite with continuous RF fields corresponding to on- and off-resonant excitations. μ^+SR was used to measure the characteristic oscillations in single-crystal $LiY_{0.95}Ho_{0.05}F_4$, and changes were observed on application of the RF fields. To model these changes, we constructed and optimized a Hamiltonian and demonstrated that it is capable of describing the experimentally observed μ^+ spin polarization. Our methodology (RF coil design, μ^+SR experiment, first-principles μ^+ stopping site calculation, and quantum evolution of the density matrix with QuTiP) opens up the possibility of performing spectroscopy experiments by varying the RF-field frequency and looking for resonances in the difference spectra. We can also envisage performing pump-probe-style experiments by using the RF field to change the state population and subsequently measuring the resulting μ^+ relaxation. Additionally, extending the RF coil design to allow microwave frequencies (0.3–30 GHz) will permit measurements of electronic (as opposed to nuclear) spin phenomena. This study paves the way for manipulating and understanding a wide variety of complex spin systems with continuous RF-μ^+SR.

We gratefully acknowledge the financial support of the UK EPSRC, Grants No. EP/S016465/1 and No. EP/N024028/1. The μ^+SR experiment was performed with the approval of the Science and Technology Facilities Council (STFC). We acknowledge the support of the Supercomputing Wales project, which is partly funded by the European Regional Development Fund (ERDF) via the Welsh government, and the facilities of the Hamilton HPC Service of Durham University. We would like to thank A. Vaidya and S. McArdle (Durham University), A. Armour (University of Nottingham), F. Flicker and E. Muljarov (Cardiff University), J. S. Lord (STFC-ISIS), and S. J. Blundell (University of Oxford) for useful discussions. Research data from this paper will be made available via [26].

*billingtond1@cardiff.ac.uk
†giblinsr@cardiff.ac.uk

[1] J. H. Brewer, S. R. Kreitzman, D. R. Noakes, E. J. Ansaldo, D. R. Harshman, and R. Keitel, Observation of muon-fluorine "hydrogen bonding" in ionic crystals, Phys. Rev. B **33**, 7813 (1986).
[2] T. Lancaster, S. J. Blundell, P. J. Baker, M. L. Brooks, W. Hayes, F. L. Pratt, J. L. Manson, M. M. Conner, and J. A. Schlueter, Muon-Fluorine Entangled States in Molecular Magnets, Phys. Rev. Lett. **99**, 267601 (2007).
[3] T. Lancaster, F. L. Pratt, S. J. Blundell, I. McKenzie, and H. E. Assender, Muon-fluorine entanglement in fluoropolymers, J. Phys. Condens. Matter **21**, 346004 (2009).
[4] S. J. Blundell, R. De Renzi, Tom Lancaster, and Francis L. Pratt, *Muon Spectroscopy: An Introduction* (Oxford University Press, New York, 2021).
[5] W. H. Zurek, Decoherence, einselection, and the quantum origins of the classical, Rev. Mod. Phys. **75**, 715–775 (2003).
[6] J. M. Wilkinson and S. J. Blundell, Information and Decoherence in a Muon-Fluorine Coupled System, Phys. Rev. Lett. **125**, 087201 (2020).
[7] J. M. Wilkinson, F. L. Pratt, T. Lancaster, P. J. Baker, and S. J. Blundell, Muon sites in PbF_2 and YF_3: Decohering environments and the role of anion Frenkel defects, Phys. Rev. B **104**, L220409 (2021).
[8] S. R. Kreitzman, D. Ll. Williams, N. Kaplan, J. R. Kempton, and J. H. Brewer, Spin Echoes for μ^+-Spin Spectroscopy, Phys. Rev. Lett. **61**, 2890 (1988).
[9] M. Iwanowski, K. Maier, J. Major, Th. Pfiz, R. Scheuermann, L. Schimmele, A. Seeger, and M. Hampele, Investigation of muon states in silicon and germanium by field-quenching and RFμSR, Hyperfine Interact. **86**, 681 (1994).
[10] S. P. Cottrell, S. F. J. Cox, J. S. Lord, and C. A. Scott, Radio-frequency μSR experiments at the ISIS pulsed muon facility, Appl. Magn. Reson. **15**, 469 (1998).
[11] N. J. Clayden, S. P. Cottrell, and I. McKenzie, Spin evolution in a radio frequency field studied through muon spin resonance, J. Magn. Reson. **214**, 144 (2012).

[12] K. W. Blazey, T. L. Estle, S. L. Rudaz, E. Holzschuh, W. Kündig, and B. D. Patterson, Double electron-muon resonance of anomalous muonium in silicon, Phys. Rev. B **34**, 1422 (1986).

[13] P. W. Percival, B. Addison-Jones, J. C. Brodovitch, and S. Sun-Mack, Radio-frequency muon spin resonance studies of endohedral and exohedral muonium adducts of fullerenes, Appl. Magn. Reson. **11**, 315 (1996).

[14] R. C. Johnson, K. H. Chen, S. R. Giblin, J. S. Lord, A. Amato, C. Baines, B. Barbara, B. Z. Malkin, and M. J. Graf, μSR study of spin dynamics in $LiY_{1-x}Ho_xF_4$, Phys. Rev. B **83**, 174440 (2011).

[15] S. R. Giblin, S. P. Cottrell, P. J. C. King, S. Tomlinson, S. J. S. Jago, L. J. Randall, M. J. Roberts, J. Norris, S. Howarth, Q. B. Mutamba, N. J. Rhodes, and F. A. Akeroyd, Optimising a muon spectrometer for measurements at the ISIS pulsed muon source, Nucl. Instrum. Methods Phys. Res., Sect. A **751**, 70 (2014).

[16] See Supplemental Material at http://link.aps.org/supplemental/10.1103/PhysRevLett.129.077201 for further details on the experiment, the first-principles μ^+ stopping site calculations, the results of fitting our model to the experimental data, and the F—μ—F eigenstates. This material includes Refs. [4,7,17–21].

[17] J. S. Möller, P. Bonfà, D. Ceresoli, F. Bernardini, S. J. Blundell, T. Lancaster, R. De Renzi, N. Marzari, I. Watanabe, S. Sulaiman, and M I Mohamed-Ibrahim, Playing quantum hide-and-seek with the muon: Localizing muon stopping sites, Phys. Scr. **88**, 068510 (2013).

[18] S. J. Clark, M. D. Segall, C. J. Pickard, P. J. Hasnip, M. I. J. Probert, K. Refson, and Mike C. Payne, First principles methods using CASTEP, Z. Kristallogr.-Cryst. Mater. **220**, 567 (2005).

[19] B. M. Huddart, A. Hernández-Melián, T. J. Hicken, M. Gomilšek, Z. Hawkhead, S. J. Clark, F. L. Pratt, and T. Lancaster, MuFinder: A program to determine and analyse muon stopping sites, arXiv:2110.07341.

[20] B. M. Huddart, MuFinder: A program to classify and analyse muon stopping sites. https://gitlab.com/BenHuddart/mufinder (2020).

[21] R. Storn and K. Price, Differential evolution: A simple and efficient heuristic for global optimization over continuous spaces, J. Global Optim. **11**, 341 (1997).

[22] J. R. Johansson, P. D. Nation, and Franco Nori, QuTiP: An open-source Python framework for the dynamics of open quantum systems, Comput. Phys. Commun. **183**, 1760 (2012).

[23] J. R. Johansson, P. D. Nation, and Franco Nori, QuTiP 2: A Python framework for the dynamics of open quantum systems, Comput. Phys. Commun. **184**, 1234 (2013).

[24] M. Gomilšek, F. L. Pratt, S. P. Cottrell, S. J. Clark, and T. Lancaster, Many-body quantum muon effects and quadrupolar coupling in solid nitrogen, arXiv:2202.05859.

[25] P. Bonfà, J. Frassineti, J. M. Wilkinson, G. Prando, M. M. Isah, C. Wang, T. Spina, B. Joseph, V. Mitrović, R. De Renzi, S. J. Blundell, and S. Sanna, Entanglement between a muon spin and $I > \frac{1}{2}$ nuclear spins, arXiv:2202.13742.

[26] D. Billington, E. Riordan, M. Salman *et al.*, FmuF quantum state manipulation research data, Cardiff University (2022), 10.17035/d.2022.0215355563.